Green Synthesis of Silver Nanoparticles Using Ionic Liquid and Application for the Detection of Dissolved Oxygen

Tsung-Hsuan Tsai, *Soundappan Thiagarajan*, *Shen-Ming Chen**

Electroanalysis and Bioelectrochemistry lab, Department of Chemical Engineering and Biotechnology, National Taipei University of Technology, No. 1, Section 3, Chung-Hsiao East Road, Taipei 106, Taiwan
*e-mail: smchen78@ms15.hinet.net

Received: August 14, 2009
Accepted: November 13, 2009

Abstract
The electrochemical synthesis of silver nanoparticles (nano-Ag) has been successfully carried out on glassy carbon electrode (GCE) and indium tin oxide electrode (ITO) using 1-butyl-3-methylimidazolium tetrafluoroborate (BMT) as green electrolytes. Further the electrodeposited nano-Ag modified ITO electrode has been examined using atomic force microscopy (AFM), and X-ray diffraction studies (XRD). The electrodeposited Ag nanoparticles on ITO were found in the size range of 5 to 35 nm. The nano-Ag film modified GCE was further coated with nafion (Nf) and BMT (1:1 ratio) mixture and found to be stable in BMT and in pH 7 phosphate buffer solution (PBS). The nano-Ag/BMT-Nf film modified GCE successfully applied for the oxygen reduction reaction in neutral pH (pH 7.0 PBS). The proposed film modified GCE successfully reduces the over potential and show well defined reduction peaks for the detection of dissolved oxygen using cyclic voltammetry (CV) and rotating disc voltammetry (RDE). The film also applied for the detection of dissolved oxygen using electrochemical impedance spectroscopic studies (EIS).

Keywords: Silver nanoparticles, Ionic liquids, Dissolved oxygen, Oxygen reduction reaction, Cyclic voltammetry

DOI: 10.1002/elan.200900410

1. Introduction

Oxygen reduction reactions are chemically and biologically important reactions. Chemically modified electrodes have been well known for the detection of important compounds [1–4]. Various types of electrodes have been reported for the electrochemical reduction of oxygen. Particularly, in physiological pH condition, the electroreduction of oxygen at mediated *Melanocarpus albomyces* laccase cathode [5], electroreduction of oxygen to water at 'wired' *Pleurotus ostreatus* laccase cathode [6], the pH-dependence of oxygen reduction on multiwalled carbon nanotube modified GCE [7], electrocatalytic reduction of oxygen on plumbagin modified GCEs were reported [8]. Next the application of nanoparticles as electrocatalyst for the oxygen reduction process has been found as interesting topic in the new era. For example, electrocatalytic reduction and determination of dissolved oxygen at the preanodized screen-printed carbon electrode modified with palladium nanoparticles [9], oxygen reduction at Au nanoparticles electrodeposited on different carbon substrates [10], gold/platinum hybrid nanoparticles supported on multi walled carbon nanotube/silica coaxial nanocables as electrocatalysts for oxygen reduction [11], gold nanoparticles dispersed into poly(aminothiophenol) as a novel electrocatalyst and evaluation of electrocatalytic activities for dioxygen reduction [12] were reported. In nanoparticles, particularly, silver has been found as a promising catalyst for the oxygen reduction reaction because of its high activity for the oxygen reduction, relatively low costs and withholds the good alcohol-tolerance capacity [13–16]. Numerous reports have been found for the chemical and electrochemical synthesis of silver nanomaterials which could be used as catalysts for the oxygen reduction reactions [17, 18], respectively.

Ionic liquids employed synthesis of nanoparticles emerged as a new interest in the field of green chemistry. Nanostructure materials have been synthesized using ionic liquids as green electrolytes. For example, green synthesis of gold nanoparticles stabilized by amine-terminated ionic liquid and their electrocatalytic activity in oxygen reduction [19] and green synthesis of highly stable platinum nanoparticles stabilized by amino-terminated ionic liquid and applied for dioxygen reduction and methanol oxidation [20] were few examples. In particular, the chemical and electrochemical synthesis of silver nanostructures using ionic liquids as green electrolytes has been found as interesting one in the green chemistry. Some of the examples are chemical synthesis of Ag and Au nanostructures like nanoparticle, cluster and nanowire formation [21], preparation of AgX (X = Cl, I) nanoparticles using ionic liquids [22], one-step synthesis of conducting polymer–noble metal nanoparticle composites using an ionic liquid [23], ionic liquids of bis(alkylethylenediamine) silver(I)) salts and the formation of silver (0) nanoparticles [24], structure and morphology controllable synthesis of Ag/carbon hybrid using ionic liquid as soft-template [25] and partially

© 2010 Wiley-VCH Verlag GmbH & Co. KGaA, Weinheim

positively charged silver nanoparticles [26] were reported. The electrodeposition of silver particles and gold nanoparticles from ionic liquid-crystal precursors [27], employing plasmas as gaseous electrodes at the free surface of ionic liquids: deposition of nanocrystalline silver particles [28], electrodeposition of silver from the 'distillable' ionic liquid [29], synthesis of silver nanoparticles in ionic liquid by a simple effective electrochemical method [30] also reported.

In this report, we attempted to fabricate the Ag nanoparticles using ionic liquid (BMT) as green electrolyte. The surface morphology of nano-Ag film modified ITO has been examined by using AFM, and X-ray diffraction studies. The nano-Ag/BMT-Nf film modified GCE successfully employed for the detection of dissolved oxygen in the neutral pH (7.0 PBS) using cyclic voltammetry and RDE techniques. The EIS technique also employed for the detection of dissolved oxygen using nano-Ag/BMT-Nf modified GCE.

2. Experimental

2.1. Reagents

1-Butyl-3-methylimidazolium tetrafluoroborate (BMT) (purum > 97%, HPLC), silver per chlorate, anhydrous, 97%, Nafion (per fluorinated ion exchange resin, 5% weight solution in lower aliphatic alcohols/H_2O mix (contains 15–20% water)) were purchased from Sigma-Aldrich (USA). All other chemicals (Merck) used were of analytical grade (99%). Double distilled deionized water was used to prepare all the solutions. A phosphate buffer solution (PBS) of pH 7.0 was prepared using Na_2HPO_4 (0.05 mol L^{-1}) and NaH_2PO_4 (0.05 mol L^{-1}).

2.2. Apparatus

All electrochemical experiments were performed using CHI 1205a potentiostats (CH Instruments, USA). The BAS GCE ($\varnothing = 0.3$ cm in diameter, exposed geometric surface area 0.07 cm^2, Bioanalytical Systems, Inc., USA) was used. A conventional three-electrode system was used which consists of an Ag/AgCl (saturated KCl) as a reference, bare or nano-Ag/BMT-Nf modified GCE as working and platinum wire as counter electrode. Particularly, for nano-Ag film deposition process ionic liquid filled (BMT) Ag electrodes (Ag/ionic liquid) has been used as the reference electrodes. For the rest of the electrochemical studies Ag/AgCl (saturated KCl) was used as a reference. Electrochemical impedance studies (EIS) were performed using ZAHNER impedance analyzer (Germany). The AFM images were recorded with multimode scanning probe microscope (Being Nano-Instruments CSPM-4000, China). The dissolved oxygen was measured using a commercial DO meter 323-A (WTW Wissenschaftlich-Technische Werkstätten GmbH, Germany). The buffer solution was entirely altered by de-aerating using nitrogen gas atmosphere. The oxygen gas was purged as required and the concentrations were measured using the commercial DO meter. The electrochemical cells were kept properly sealed to avoid the oxygen interference from the atmosphere. For our convenience, indium tin oxide (ITO) thin film coated glass electrodes have been used for the AFM analysis.

2.3. Fabrication of Nano-Ag Film

Prior to the electrochemical deposition process, the GCE was well polished with the help of BAS polishing kit with aqueous slurries of alumina powder (0.05 μm), rinsed and ultrasonicated in double distilled deionized water. The GCE was electrodeposited with silver nanoparticles by performing in 1 mL BMT containing 1 mM $AgClO_4$ and the potential cycling between 1.2 and 0 V at the scan rate of 0.05 V/s for three cycles. Figure 3A shows the cyclic voltammograms of the electrochemical deposition process of nano-Ag film on GCE. The anodic oxidation of Ag occurs at 0.69 V and cathodic reduction occurs 0.39 V. Continuous cycling and growth of the corresponding peaks validates the deposition of Ag nanoparticles on the GCE surface. Further the silver nanoparticles modified GCE was washed with deionized water and dried for 5 minutes. To prevent the easy oxidation of Ag nanoparticles, the nano-Ag modified GCE surface has been coated with 4 μL of nafion and ionic liquid (BMT) mixture (ratio (1:1)) and dried in air and kept in refrigerator for 2 hours at 4 °C. Further the nano-Ag/BMT-Nf modified GCE has been employed in BMT for different scan rate studies. Surface cleaned ITO glass electrode has been immersed in 1 mL BMT containing 1 mM $AgClO_4$ (potential cycling between 1.2 and 0 V at the scan rate of 0.05 V/s for three cycles) for the electrodeposition of Ag nanoparticles.

3. Results and Discussion

3.1. AFM Analysis

The surface morphology of electrodeposited Ag nanoparticles has been examined using AFM. Here the AFM studies could furnish the comprehensive information about the surface morphology of nano-Ag on the ITO surface. The AFM parameters have been evaluated for 1400 × 1400 nm surface area. The surface morphology of nano-Ag film was examined by using the tapping mode (Fig. 1A). Figures 1A and B show the 2D and 3D magnified view of the electrodeposited nano-Ag film (3 cycles) on ITO. Figure 1C and D shows the cross-sectional and granularity normal distribution chart of Ag nanoparticles electrodeposited on ITO surface. From Figure 1A, we can see the existence of Ag nanoparticles in obvious manner with the average size range of 5 to 35 nm. The other amplitude parameters such like roughness average (*sa*) for nano-Ag film (1400 × 1400 nm) was found as 1.96 nm. The root mean square roughness was found as 2.91 nm. By using the combination of skewness and kurtosis values, it is possible to identify the film surfaces

www.spm.com.cn

 © 2010 Wiley-VCH Verlag GmbH & Co. KGaA, Weinheim

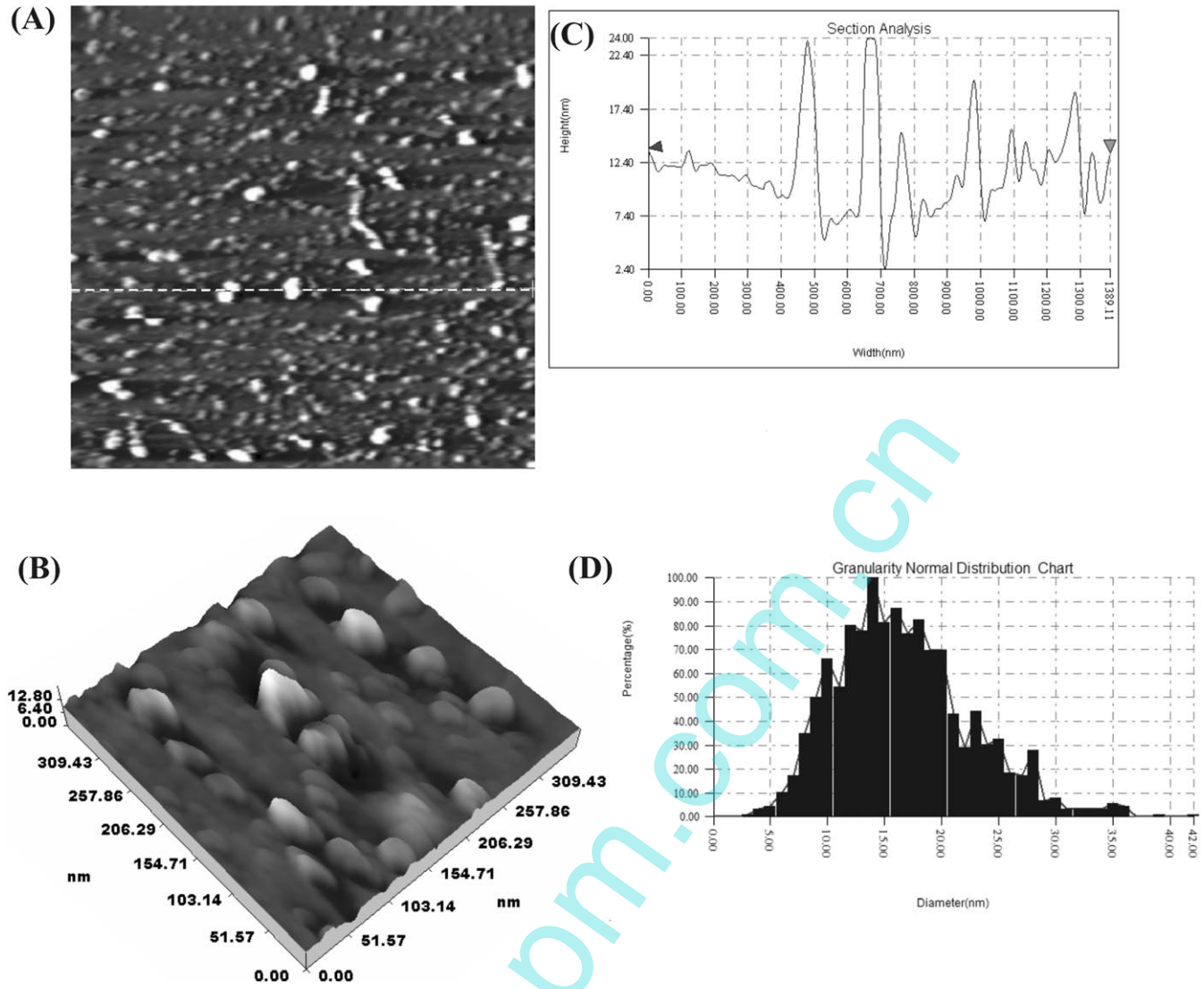

Fig. 1. Tapping mode AFM image of electrodeposited nano-Ag film on ITO (3 cycles). (A) Topographic (2D), (B) magnified three dimensional views (3D) of nano-Ag film on ITO. (C) Cross-sectional analysis graph and (D) granularity normal distribution chart for the nano-Ag film.

which have relatively flat top and deep valleys. The skewness (R_{sk}) measures the symmetry of variation of the surface about its mean plane. Positive skewness value (1.58) obtained for nano-Ag film shows that the surface comprised of disproportionate number of peaks which indicates that the Ag nanoparticles were unevenly allocated on the ITO surface. Next, the kurtosis (R_{ku}) is a measure of the unevenness or sharpness of the surface. A surface that is centrally distributed has a kurtosis value greater than 3. In this film, the kurtosis value was found as 7.26. Based on the height normal distribution chart for nano-Ag film (Figure not shown) average height of the Ag nanoparticle is found as 4.5 nm. However, maximum number of Ag nanoparticles exhibited in 2.0 nm height, respectively.

The granularity normal distribution chart (Fig. 1D) shows that the average diameter of silver nanoparticles has been found as 16.1 nm. In particular, the maximum number of particles has been found in the size range of 14 nm. The total number of Ag nanoparticles found for the 1400×1400 nm surface area was 1078. Further the electrodeposition process of the nano-Ag film has been optimized by varying the concentration and scan rates. All these variation studies have been examined using AFM and shown in Table 1. For the increasing concentration and scan cycles the size of the nanoparticles falls in the higher dimensional size ranges, respectively. Therefore, for the application process we have followed three cycles (0.05 V/s) as optimized deposition condition for the fabrication of Ag nanoparticles. Finally the above AFM results clearly illustrate the surface nature of the nano-Ag film on the ITO.

3.2. XRD Analysis

XRD has been employed to validate the proposed Ag nanoparticles structure on the ITO. Figure 2 shows the XRD

www.spm.com.cn

Table 1. AFM analysis table for the Ag nanoparticles deposition process by varying the solution concentration and number of cycles.

S. No	Concentration of $AgClO_4$ in 1 mL BMT	No of cycles (scan rate 0.05 V/s)	Average diameter of the Ag nanoparticles
1	1×10^{-3} M	3	16.1
		6	42.3
		9	115.3
2	5×10^{-3} M	3	141.3
		6	108.7
		9	139.6
3	1×10^{-2} M	3	78.3
		6	95.6
		9	103.5

patterns obtained for the Ag nanoparticles on ITO surface. Three different and important characteristic peaks obtained for the electrodeposited Ag nanoparticles. They are, 38.14 (111), 44.30 (200) and 64.51 (220). The remaining peak pattern corresponds to the ITO surface. This three peaks (38.14 (111), 44.30 (200) and 64.51 (220)) validate the presence of Ag nanoparticles. Based on this XRD pattern we propose that the electrodeposited Ag nanoparticles possess the face centered cubic structure (fcc) [21, 31, 32]. Finally, based on this XRD analysis the nanostructure of the silver particles has been verified.

3.3. Characterization of Nano-Ag/BMT-Nf Film Modified GCE

The influence of scan rate on the electrochemical response of nano-Ag/BMT-Nf modified GCE in BMT was investigated. Cyclic voltammetry was performed for the different scan rate studies. Figure 3B represents the cyclic voltammograms of nano-Ag/BMT-Nf film modified GCE in BMT at different scan rates. In the 1.2 to 0 V potential range the nano-Ag/ BMT-Nf film exhibits one sharp anodic peak and broad cathodic peak at 0.56 and 0.32 V, respectively. The anodic and cathodic peak current increases linearly with respect to the scan rate in the range from 0.01 to 1 V/s. The scan rate also affects on both the anodic and cathodic peak current peak positions. For the increasing scan rate, the anodic peak current was decreasing. At the same time, the cathodic peak current becomes much broader in the higher scan rates. The inset of Figure 3B shows the plot of anodic and cathodic peak current vs. scan rate. The corresponding linear regression equations were found as I_{pc} (μA) = 6.565v (V/s) − 0.024, $R^2 = 0.996$ and I_{pa} (μA) = 2.649 v (V/s) + 0.945, $R^2 = 0.972$. Linear increase in the anodic and cathodic peak currents of nano-Ag/BMT-Nf film according to the scan rate illustrates that the film was typical characteristic of surface controlled thin-layer electrochemical behavior, respectively.

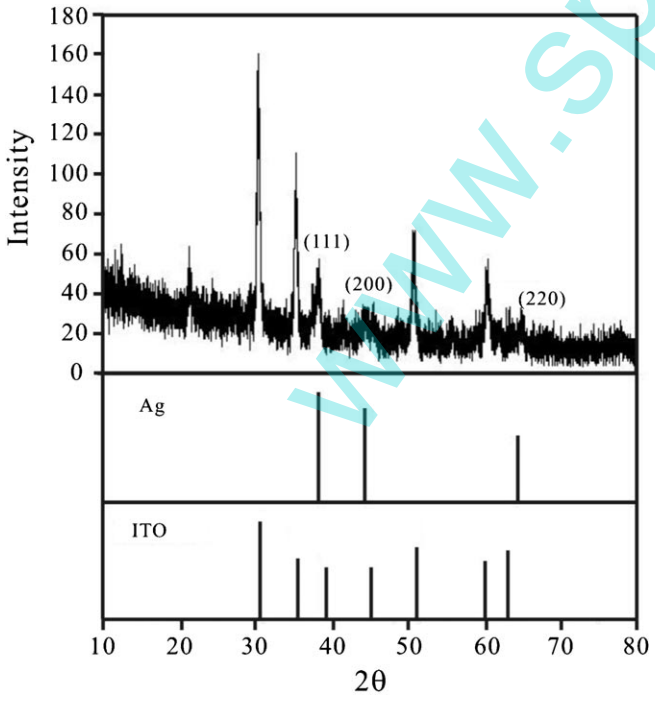

Fig. 2. X-ray diffraction pattern of nano-Ag film on ITO.

3.4. EIS Analysis

The electrochemical activity of nano-Ag/BMT-Nf modified GCE has been examined using EIS technique. Impedance spectroscopy is an effective method to probe the features of surface modified electrodes. This study was employed to analyze detailed electrochemical activities of modified electrode with individual or mixed components. The complex impedance can be presented as a sum of the real, $Z'(\omega)$, and imaginary $Z''(\omega)$, components that originate mainly from the resistance and capacitance of the cell. From the shape of an impedance spectrum, the electron-transfer kinetics and diffusion characteristics can be extracted. The respective semicircle parameters correspond to the electron transfer resistance (R_{et}) and the double layer capacity (C_{dl}) nature of the modified electrode. Figure 4 shows the Faradaic impedance spectra, presented as Nyquist plots (Z'' vs. Z') for the nano-Ag film, nano-Ag/BMT-Nf film modified GCE and bare GCE. The bare GCE exhibits almost a straight line (a) with a very small depressed semi

www.spm.com.cn

 © 2010 Wiley-VCH Verlag GmbH & Co. KGaA, Weinheim

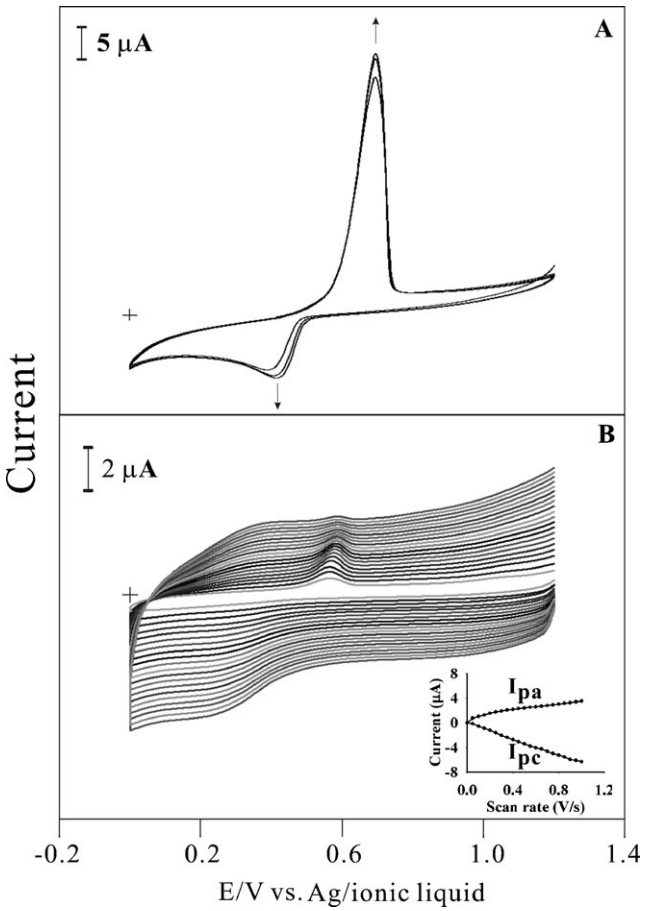

Fig. 3. (A) Consecutive cyclic voltammograms of Ag nanoparticles deposition process on GCE using 1 mL BMT containing 1 mM $AgClO_4$ in the potential range of 1.2 to 0 V (scan rate: 0.05 V/s) for 3 three cycles. (B) Different scan rate study of nano-Ag/BMT-Nf film modified GCE in BMT. Scan rate in the range of 0.01 – 1 V/s. Inset: plot of anodic and cathodic peak current vs. scan rate.

circle arc ($R_{et} = 0.83$ (Z'/kΩ)) represents the characteristics of diffusion limited electron-transfer process on the electrode surface. At the same time, the nano-Ag film modified GCE shows like a depressed semi circle arc with an interfacial resistance due to the electrostatic repulsion between the charged surface and probe molecule Fe $(CN)_6^{3-/4-}$ (b). This depressed semicircle arc ($R_{et} = 0.49$ (Z'/kΩ)) clearly indicates the lower electron transfer resistance behavior comparing with the bare GCE. At the same time, the nano-Ag/BMT-Nf film modified GCE's R_{et} has been found as 1.16 (Z'/kΩ). The increase in the value of electron transfer resistance (R_{et}) due to the coating of BMT and nafion as a bilayer on the nano-Ag film modified GCE surface. Thus, the electron transfer process will become as a slow process on the nano-Ag/BMT-Nf film modified GCE. Finally, these results clearly illustrate the electrochemical activities of the nano-Ag and nano-Ag/BMT-Nf film modified GCEs, respectively.

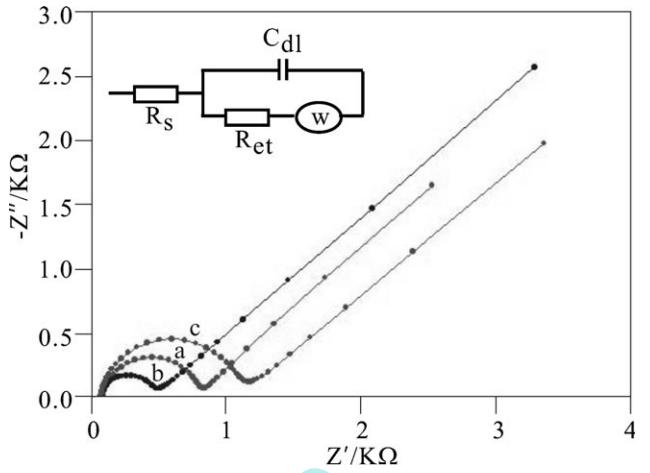

Fig. 4. Electrochemical impedance spectra of (a) bare GCE, (b) nano-Ag film and (c) nano-Ag/BMT-Nf film modified GCE in pH 7.0 PBS containing 5×10^{-3} M $[Fe(CN)_6]^{-3/-4}$ (Amplitude: 5 mV).

3.5. Electrocatalytic Reduction of Dissolved Oxygen at Nano-Ag/BMT-Nf Modified GCE

Figure 5A shows the cyclic voltammograms of nano-Ag/BMT-Nf modified GCE in the presence of oxygen saturated solution. The amount of dissolved oxygen was measured by using commercially available oxygen meter. Figure 5A shows the cyclic voltammograms of nano-Ag/BMT-Nf modified GCE in a pH 7.0 PBS solution in the presence of various concentrations of dissolved oxygen. As it can be seen in Figure 5A, a single reduction peak at – 0.44 V can be observed in the pH 7.0 PBS solution for the oxygen reduction reaction. Further it can be noticed that there is a great increase in the cathodic peak current at nano-Ag/BMT-Nf film modified GCE for the increasing concentrations of dissolved oxygen in pH 7.0 PBS (Fig. 5A, curves a – i). Here the increasing reduction peak current clearly shows the electrocatalytic activity of the nano-Ag/BMT-Nf film modified GCE surface. The catalytic peak potential for the oxygen reduction is found at – 0.44 V for nano-Ag/BMT-Nf film modified GCE, whereas for the bare GCE it fails to exhibit reduction peak for the dissolved oxygen and shows a small diminished peak at around – 0.81 V. Also, the cathodic peak current of nano-Ag/BMT-Nf film modified GCE is increasing along with the increasing concentrations of the dissolved oxygen in pH 7.0 PBS. Therefore, a decrease of about – 0.37 V in over potential and the significant enhancement of the reduction peak current is achieved with the nano-Ag/BMT-Nf modified GCE. This result is a clear indication for the occurrence of electrocatalytic reduction of dissolved oxygen at the nano-Ag/BMT-Nf modified GCE. The inset of Figure 5A shows the reduction peak current vs. concentration plot for the electrocatalytic reduction of dissolved oxygen. The calibration plot resulted as linear one with the linear regression equation of I_{pc} (μA) = 3.4382 C (mg/L) – 0.3982, with a correlation coefficient of $R^2 =$ 0.9962.

www.spm.com.cn

 © 2010 Wiley-VCH Verlag GmbH & Co. KGaA, Weinheim

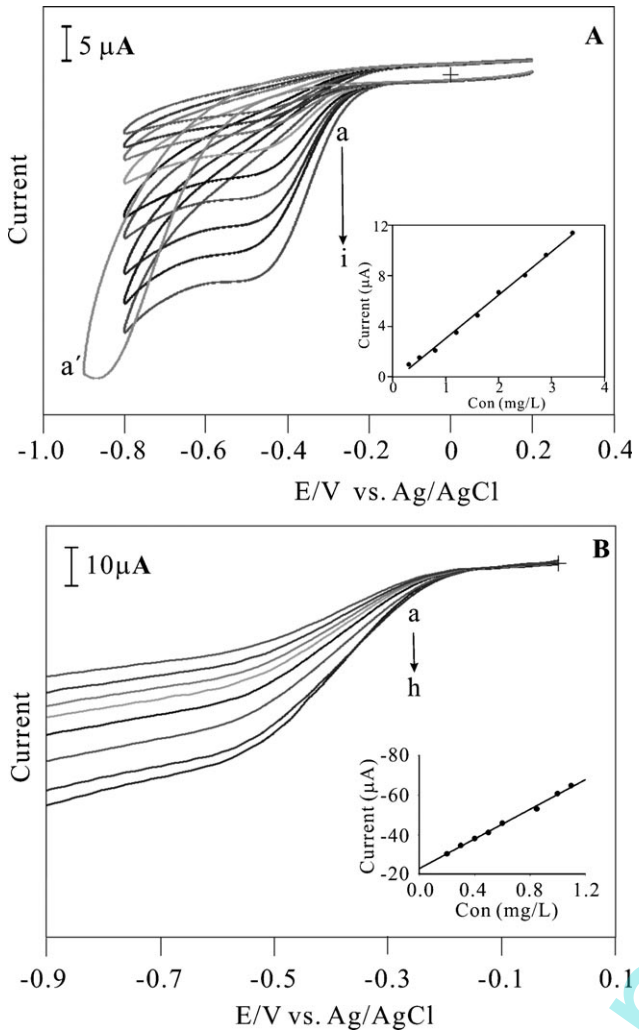

Fig. 5. (A) Cyclic voltammograms of nano-Ag/BMT-Nf film for the detection of dissolved oxygen in pH 7.0 PBS. Dissolved oxygen concentrations were in the range of (a – i): 0.3, 0.5, 0.8, 1.2, 1.6, 2, 2.5, 2.9, and 3.4 mg/L, (a′) bare GCE = 3.4 mg/L (scan rate: 0.1 V/s). Inset: calibration plot of reduction current vs. concentration of dissolved oxygen. (B) RDE voltammograms of nano-Ag/BMT-Nf film for the detection of dissolved oxygen in pH 7.0 PBS. Dissolved oxygen concentration were in the range of (a – h): 0.2, 0.3, 0.4, 0.5, 0.6, 0.85, 1.0, and 1.1 mg/L. Inset: calibration plot of reduction current vs. concentration of dissolved oxygen.

Next the RDE technique was employed for the detection of dissolved oxygen in pH 7.0 PBS. The nano-Ag/BMT-Nf film modified GCE rotation speed was set to be as 600 rpm and the reduction progress has been examined within the potential range of 0 to − 0.9 V (Fig. 5B). For the increasing concentrations of dissolved oxygen, the reduction peak current increases at the nano-Ag/BMT-Nf film modified GCE. The reduction peak current vs. concentration of the dissolved oxygen has been plotted and shown in the Inset of Figure 5B. The calibration plot resulted as linear one for the 0.2 to 1.1 mg/L concentration range. The from this calibration plot the linear regression equation was expressed as I_{pc} (μA) = − 37.45 C (mg/L) − 1.058, with a correlation coefficient of $R^2 = 0.999$. These result clearly indicates the electrocatalytic oxygen reduction occurs at the nano-Ag/BMT-Nf film modified GCE. The electrocatalytic reduction of dissolved oxygen has been compared with bare Ag electrode. Figure 6 shows the CV response of bare Ag electrode and nano-Ag/BMT-Nf film modified GCE for the electrocatalytic reduction of dissolved oxygen. At the Ag electrode, the oxygen reduction appears as sharp peak at around − 0.8 V. At the same time, nano-Ag/BMT-Nf film reduces the over potential and the corresponding peak appears at − 0.44 V. This shows that the proposed film is more suitable for the detection of dissolved oxygen comparing with the bare Ag electrode. Furthermore the obtained result is comparable one with previous literature reports, respectively (Table 2).

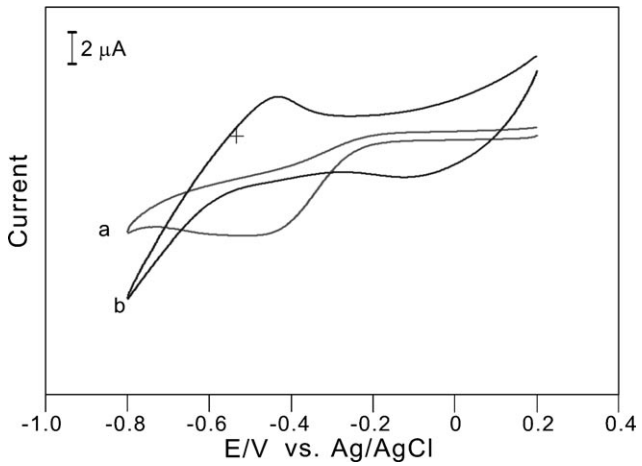

Fig. 6. (A) Cyclic voltammetric response for the detection of dissolved oxygen (0.8 mg/L) at bare Ag electrode (curve a) and nano-Ag/BMT-Nf film modified GCE (curve b).

Table 2. Comparison table for the oxygen reduction reaction. PBS: phosphate buffer solution; SWNT: single-walled carbon nanotubes; AB: acetylene black; UPD: under potential deposition

Type of film	Solution (pH)	Oxygen reduction potential (V)	Reference
GCE/Au-Ag alloy nanoparticles	(7.2)	− 0.55 [a]	[33]
Ag-deposited microelectrode	0.01 M KCl	− 0.4	[34]
GCE/(Ag-MnO_2)/SWNT/Nafion	1 M KOH	− 0.4 [a]	[35]
GCE/(Ag-MnO_2)/AB/Nafion			
Au(111)/Ag-UPD	0.5 M KOH	− 0.4	[36]
GCE/nano-Ag/BMT-Nf film	PBS (7.0)	− 0.44	This work

[a] approximate value

 © 2010 Wiley-VCH Verlag GmbH & Co. KGaA, Weinheim

www.cnki.com.cn

3.6. Impedimetric Detection of Dissolved Oxygen at Nano-Ag/BMT-Nf Modified GCE

Figure 7 shows the Nyquist curves obtained for the specific response of dissolved oxygen detection and adsorption at the nano-Ag/BMT-Nf modified GCE. The plot of real component (Z') and the imaginary component Z'' (imaginary) resulted in the formation of a depressed semicircular Nyquist plot. This type of impedance spectrum is an analytic of a surface modified electrode system where the electron transfer is slow and the impedance is controlled by the interfacial electron transfer at high frequency. Open circuit potential was applied for this investigation. The concentration range of oxygen dissolved was measured using the commercially available oxygen meter. The electron-transfer resistance (R_{et}) changes from the baseline response for every each increasing concentrations of dissolved oxygen, R_{et} vs. dissolved oxygen concentration (mg/L) and calibration plot shown in the inset of Figure 7. The electron-transfer resistance increases with the increasing concentrations of dissolved oxygen which gives rise to a linear-type detection response in the range of 0.2 to 1.1 mg/L. The depressed semicircular arc diameter increases upon the increasing concentration of dissolved oxygen indicates the increasing concentration of oxygen hinders the electron transfer process and increases the electron transfer resistance of the corresponding film, respectively. Several models were attempted and best fit for the data has been used. Up to 1.1 mg/L the experimental data fitted and the regression equation obtained for the detection of dissolved oxygen at the nano-Ag/BMI-Nf film modified GCE was R_{et} (kΩ) = 1.745 C (mg/L) + 0.888, with a correlation coefficient of $R^2 = 0.988$. Finally, this result clearly explicates the possible impedimetric detection of oxygen reduction using nano-Ag/BMT-Nf modified GCE.

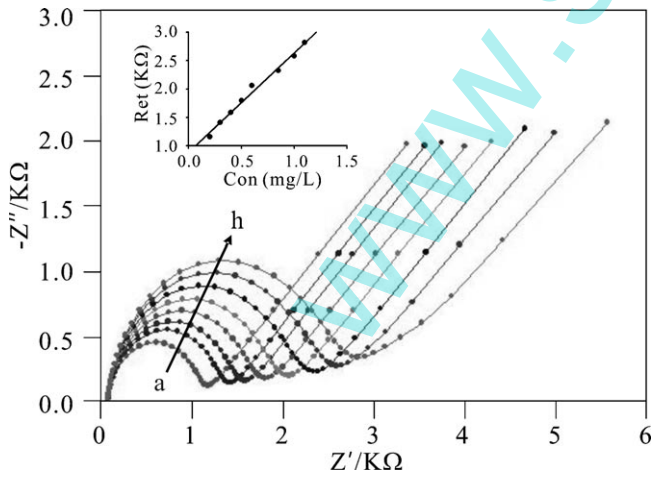

Fig. 7. Nyquist plot response of nano-Ag/BMT-Nf film modified GCE for the various concentrations of dissolved oxygen in pH 7.0 PBS containing 5×10^{-3} M $[Fe(CN)_6]^{-3/-4}$. The dissolved oxygen concentrations were in the range of (a – h): 0.2, 0.3, 0.4, 0.5, 0.85, 1.0, and 1.1 mg/L. Inset: Calibration plot of ΔR_{et} vs. concentration of dissolved oxygen.

4. Conclusions

Here we report a simple method for the electrochemical fabrication of stable Ag nanoparticles (using ionic liquid (BMT) as green electrolytes) modified GCE and ITO. The electrodeposited nano-Ag film has been characterized by using AFM and X-ray diffraction studies. The nano-Ag/BMT-Nf film modified GCE was found to be effective for oxygen reduction reactions in neutral pH conditions. Overall, the proposed film is very easy to fabricate using ionic liquids as green electrolytes, ecofriendly and could be applied to various types of oxygen reduction reaction related studies.

5. Acknowledgements

This work was supported by The National Science Council of Taiwan (ROC). We acknowledge our thanks to Dr. R. Thangamuthu, post doctoral fellow for his fruitful discussion for revising this manuscript.

6. References

[1] R. W. Murray, *Ann. Rev. Mater. Sci* **1984**, *14*, 145.
[2] R. W. Murray, A. G. Ewing, R. A. Durst, *Anal. Chem.* **1987**, *59*, 379A.
[3] P. Shakkthivel, S.-M. Chen, *Biosens. Bioelectron.* **2007**, *22*, 1680.
[4] S. Thiagarajan, T.-H. Tsai, S.-M. Chen, *Biosens. Bioelectron.* **2009**, *24*, 2712.
[5] P. Kavanagh, P. Jenkins, D. Leech, *Electrochem. Commun.* **2008**, *10*, 970.
[6] S. C. Barton, M. Pickard, R. V. Duhal, A. Heller, *Biosens. Bioelectron.* **2002**, *17*, 1071.
[7] I. Kruusenberg, N. Alexeyeva, K. Tammeveski, *Carbon* **2009**, *47,* 651.
[8] M. M. Ardakani, P. E. Karami, H. R. Zare, M. Hamzehloo, *Microchim. Acta* **2007**, *159,* 165.
[9] C.-C. Yang, A. Senthil Kumar, J.-M. Zen, *Electroanalysis* **2006**, *18*, 64.
[10] M. S. El-Deab, T. Sotomura, T. Ohsaka, *Electrochim. Acta* **2006**, *52*, 792.
[11] S. Guo, S. Dong, E. Wang, *J. Phys. Chem. C* **2008**, *112*, 2389.
[12] A. I. Gopalan, K.-P. Lee, K. M. Manesh, P. Santhosh, J. H. Kim, *J. Mol. Catal. A, Chem.* **2006**, *256*, 335.
[13] M. Lefevre, J. P. Dodelet, *Electrochim. Acta* **2003**, *48*, 2749.
[14] F. H. B. Lima, J. F. R. de Castro, E. A. Ticianelli, *J. Power Sources* **2006**, *161*, 806.
[15] H. Meng, P. K. Shen, *Electrochem. Commun.* **2006**, *8*, 588.
[16] B. B. Blizanac, P. N. Ross, N. M. Markovic, *Electrochim. Acta* **2007**, *52*, 2264.
[17] K. Ni, L. Chen, G. Lu, *Electrochem. Commun.* **2008**, *10*, 1027.
[18] L. Demarconnay, C. Coutanceau, J.-M. Léger, *Electrochim. Acta* **2004**, *49*, 4513.
[19] Z. Wang, Q. Zhang, D. Kuehner, A. Ivaska, L. Niu, *Green Chem.* **2008**, *10*, 907.
[20] F. Li, F. Li, J. Song, J. F. Song, D. Han, L. Niu, *Electrochem. Commun.* **2009**, *11*, 351.
[21] A. I. Bhatt, A. Mechler, L. L. Martin, A. M. Bond, *J. Mater. Chem.* **2007**, *17*, 2241.

www.spm.com.cn

[22] E. Rodil, L. Aldous, C. Hardacre, M. C. Lagunas, *Nanotechnology* **2008**, *19*, 105603.
[23] J. M. Pringle, O. W. Jensen, C. Lynam, G. G. Wallace, M. Forsyth, D. R. MacFarlane, *Adv. Funct. Mater.* **2008**, *18*, 2031.
[24] M. Iida, C. Baba, M. Inoue, H. Yoshida, E. Taguchi, H. Furusho, *Chem. Eur. J.* **2008**, *14*, 5047.
[25] S. Y. Wu, Y. S. Ding, X. M. Zhang, H. O. Tang, L. Chen, *J. Solid State Chem*. **2008**, *181*, 2171.
[26] S. W. Kang, K. Char, Y. S. Kang, *Chem. Mater.* **2008**, *20*, 1308.
[27] W. Dobbs, J.-M. Suisse, L. Douce, R. Welter, *Angew. Chem. Int. Ed.* **2006**, *45*, 4179.
[28] S. A. Meiss, M. Rohnke, L. Kienle, S. Z. Abedin, F. Endres, J. Janek, *ChemPhysChem* **2007**, *8*, 50.
[29] A. I. Bhatt, A. M. Bond, *J. Electroanal. Chem*. **2008**, *619*, 1.
[30] N. Li, X. Bai, S. Zhang, Y. Gao, L. Zheng, J. Zhang, H. Ma, *J. Dispers. Sci. Tech.* **2008**, *29*, 1059.
[31] D. Dorjnamjin, M. Ariuna, Y. K. Shim, *Int. J. Mol. Sci.* **2008**, *9*, 807.
[32] S. Wu, Y. Ding, X. Zhang, H. Tang, *Mater. Lett.* **2008**, *62*, 3301.
[33] S. Devarajan, P. Bera, S. Sampath, *J. Colloid Interf. Sci.* **2005**, *290*, 117.
[34] Y.-P. Chen, S.-Y. Liu, F. Fang, S.-H. Li, G. Liu, Y.-C. Tian, Y. Xiong, H.-Q. Yu, *Environ. Sci. Technol.* **2008**, *42*, 8465.
[35] F.-P. Hu, X.-G. Zhang, F. Xiao, J.-L. Zhang, *Carbon* **2005**, *43*, 2931.
[36] A. Kongkanand, S. Kuwabata, *Electrochem. Commun.* **2003**, *5*, 133.

www.spm.com.cn

 © 2010 Wiley-VCH Verlag GmbH & Co. KGaA, Weinheim